Title

Spatially resolved multicolor $CsPbX_3$ nanowire heterojunctions via anion exchange.

Journal

Proceedings of the National Academy of Sciences of the United States of America, 114(28)

ISSN

0027-8424

Authors

Dou, Letian
Lai, Minliang
Kley, Christopher S
et al.

Publication Date

2017-07-01

DOI

10.1073/pnas.1703860114

Peer reviewed

Spatially resolved multicolor $CsPbX_3$ nanowire heterojunctions via anion exchange

Letian Dou[a,b,1], Minliang Lai[a,1], Christopher S. Kley[a,1], Yiming Yang[a,b], Connor G. Bischak[a], Dandan Zhang[a], Samuel W. Eaton[a], Naomi S. Ginsberg[a,b,c,d,e], and Peidong Yang[a,b,d,f,2]

[a]Department of Chemistry, University of California, Berkeley, CA 94720; [b]Materials Sciences Division, Lawrence Berkeley National Laboratory, Berkeley, CA 94720; [c]Department of Physics, University of California, Berkeley, CA 94720; [d]Kavli Energy NanoSciences Institute, Berkeley, CA 94720; [e]Molecular Biophysics and Integrative Bioimaging Division, Lawrence Berkeley National Laboratory, Berkeley, CA, 94720; and [f]Department of Materials Science and Engineering, University of California, Berkeley, CA 94720

This contribution is part of the special series of Inaugural Articles by members of the National Academy of Sciences elected in 2016.

Contributed by Peidong Yang, May 29, 2017 (sent for review March 8, 2017; reviewed by Liberato Manna, Cun-Zheng Ning, and Qihua Xiong)

Halide perovskites are promising semiconductor materials for solution-processed optoelectronic devices. Their strong ionic bonding nature results in highly dynamic crystal lattices, inherently allowing rapid ion exchange at the solid–vapor and solid–liquid interface. Here, we show that the anion-exchange chemistry can be precisely controlled in single-crystalline halide perovskite nanomaterials when combined with nanofabrication techniques. We demonstrate spatially resolved multicolor $CsPbX_3$ (X = Cl, Br, I, or alloy of two halides) nanowire heterojunctions with a pixel size down to 500 nm with the photoluminescence tunable over the entire visible spectrum. In addition, the heterojunctions show distinct electronic states across the interface, as revealed by Kelvin probe force microscopy. These perovskite heterojunctions represent key building blocks for high-resolution multicolor displays beyond current state-of-the-art technology as well as high-density diode/transistor arrays.

nanowire | halide perovskite | anion exchange | heterojunction

Significant research efforts are currently directed toward lead halide-based perovskites, owing to their unusual optoelectronic and photovoltaic properties (1–5). In addition to polycrystalline thin films, various solution-based synthetic routes toward low-dimensional nanostructures of halide perovskites have been recently demonstrated, with control over size, shape, mixed halide composition, and consequently their band gap and emission wavelength (6–10). Interestingly, it has been shown that these materials, both in bulk and in nanocrystalline form, can undergo fast anion-exchange reactions at the solid–liquid or solid–gas interface, with a fine-tuning of the chemical composition and electronic properties (11–14). The fast ion-exchange kinetics in halide perovskite are related to the low defect formation energy and the existence of a large number of vacancies, which make the ions highly mobile in the crystal lattice (15). As a result, the anion-exchange reaction in halide perovskites favors forming homogeneous alloys instead of any kind of heterostructures as commonly observed in II–VI semiconductor compounds. If the exchange reaction can be localized at particular positions, then it is possible to produce substrates with well-defined patterns of semiconductor heterojunctions (16–20). The physical properties (optical, electrical, magnetic, etc.) of the heterostructure are fundamentally interesting, and the patterned semiconductor heterojunctions are essential for the fabrication of large-scale high-density integrated electronic and photonic devices.

Compared with perovskite polycrystalline thin films and quantum dots, single-crystalline nanowires provide an ideal platform for producing and studying heterojunctions via ion-exchange chemistry because of the absence of grain boundaries and the unique one-dimensional geometry (21–24). The relatively thin diameter of the nanowire ensures rapid ion exchange in the radial direction, whereas the micrometer scale length creates a natural channel for studying the optical and electrical properties of the junction. Moreover, a relatively small cross-sectional area makes the nanowire more tolerant to interfacial strain that is induced by crystal lattice mismatch (composition change) across the junction. Furthermore, advanced functionality can be achieved by creating multiple junctions within a single nanowire. Here, we demonstrate spatially resolved $CsPbX_3$ (X = Cl, Br, I, or alloys of two halides) semiconductor nanowire heterojunctions with a pixel size down to 500 nm and multiple emission colors. Selected area anion exchange from cesium lead bromide to cesium lead chloride or iodide is achieved at high spatial resolution by defining a reaction window with high spatial resolution using electron-beam (e-beam) lithography. A sharp junction is observed, with distinct optical and electronic properties across the heterojunction interface. Intricate patterns on $CsPbBr_3$ plates were also fabricated successfully by this method.

Results and Discussion

$CsPbBr_3$ nanowires as well as some thin plates were grown using our previously reported solution-based method (25, 26). The diameter of a typical nanowire is several hundreds of nanometers with a length of up to 30 micrometers (*SI Appendix*, Fig. S1). To study the anion-exchange chemistry on the single-nanowire level, individual $CsPbBr_3$ nanowires were picked using a micromanipulator

Significance

Semiconductor heterojunction is a key building block in modern electronics and optoelectronics. The accurate control over the composition, band gap, energy level (band bending), and doping level is the foundation of ideal functional heterojunctions. We demonstrate highly spatially resolved heterojunctions in a type of semiconductor, halide perovskites, which show great potential in photovoltaic and solid-state lighting applications. We accomplish this through the combination of facile anion-exchange chemistry with nanofabrication techniques. The halide perovskite nanowire heterojunction provides an ideal platform for fundamental studies and technological applications. For example, multicolor lasers or LEDs could be made using such localized heterojunctions; quantitative interdiffusion and ion migration dynamics could be examined at elevated temperatures, etc.

Author contributions: L.D., M.L., and P.Y. designed research; L.D., M.L., C.S.K., Y.Y., C.G.B., D.Z., and S.W.E. performed research; L.D., M.L., C.S.K., N.S.G., and P.Y. analyzed data; and L.D., C.S.K., N.S.G., and P.Y. wrote the paper.

Reviewers: L.M., Istituto Italiano di Tecnologia; C.-Z.N., Arizona State University; and Q.X., Nanyang Technological University.

Conflict of interest statement: P.Y. and Cun-Zheng Ning are coauthors on a 2016 review article.

[1]L.D., M.L., and C.S.K. contributed equally to this work.

[2]To whom correspondence should be addressed. Email: p_yang@berkeley.edu.

This article contains supporting information online at www.pnas.org/lookup/suppl/doi:10.1073/pnas.1703860114/-/DCSupplemental.

and transferred to a clean SiO_2/Si substrate. A droplet of reaction solution containing oleylammonium chloride in 1-octadecene was used to cover the nanowire on the substrate. The reaction was in situ examined under a microscope with a 325-nm laser excitation. As shown in *SI Appendix*, Fig. S2, during the reaction period (~12 h), the photoluminescence (PL) of the nanowire gradually blue-shifted, without the coexistence of both green and purple–blue emission, respectively, from pure $CsPbBr_3$ and $CsPbCl_3$, indicating the formation of homogeneous $CsPbX_3$ alloys instead of any Br^-- or Cl^--rich domains. For cesium lead halide perovskites, the reaction probably occurs via a vacancy-assisted diffusion mechanism (12), and the anion-exchange reaction zone width is probably close to the crystal size (27), which leads to alloy formation instead of a core–shell structure. The reaction dynamics are important for controlling the conversion degree and therefore the optical and electronic properties of the nanowire. The mild reaction conditions we developed here are essential for maintaining the nanowire morphology and compatible with nanofabrication processes.

Next, we studied the anion-exchange chemistry on the partially masked nanowires for creating spatially well-defined heterojunctions. As shown in Fig. 1*A*, after transferring the nanowire, a thin layer of poly(methyl methacrylate) (PMMA) was spin-cast.

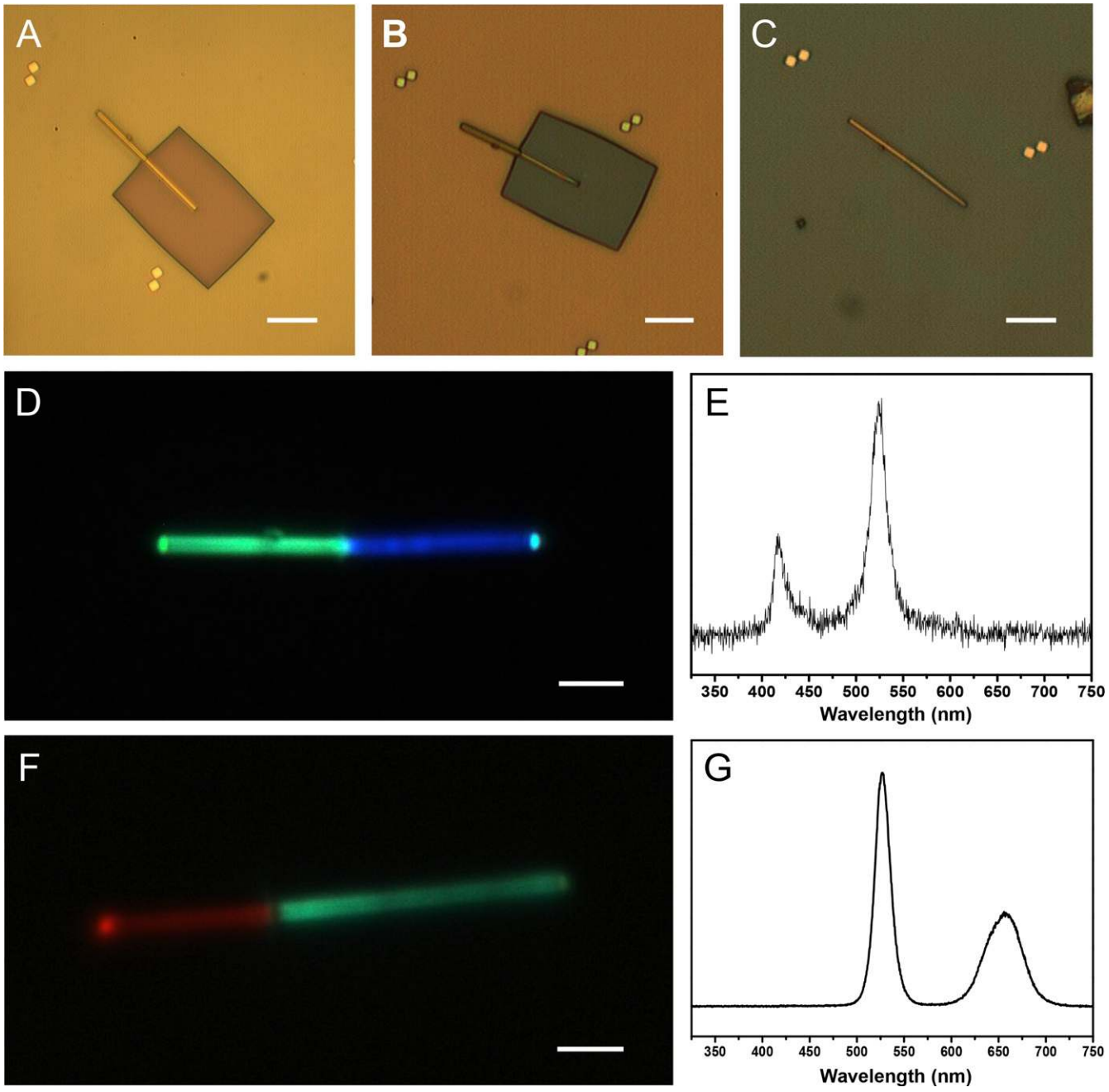

Fig. 1. Cesium lead halide perovskite nanowire heterojunctions fabrication and PL characterization. (*A*) Optical microscope image of a $CsPbBr_3$ nanowire partially coated with PMMA. The square-shaped opening was created by EBL. (*B*) The $CsPbBr_3$ nanowire partially coated with PMMA after anion exchange. (*C*) The $CsPbBr_3$ nanowire after anion exchange and after removal of PMMA. (*D*) Optical images of the partial bromide partial chloride nanowire under laser excitation. (*E*) The corresponding PL emission spectrum. (*F*) Optical images of the partial bromide partial iodide nanowire under laser excitation. (*G*) The corresponding PL emission spectrum. (Scale bars, *A*–*C*, 10 μm.) (Scale bars, *D* and *F*, 3 μm.)

A designated area of the PMMA was removed using e-beam lithography to expose part of the nanowire. Then the substrate was dipped into an oleylammonium halide (OAmX, X = Cl, I) solution. During the reaction, the PMMA layer remains intact as shown in Fig. 1*B*. After the anion-exchange reaction, the PMMA layer was completely removed by washing with chlorobenzene and hexanes, as shown in Fig. 1*C*. Details and a schematic illustration of the fabrication process can be found in *SI Appendix*, Fig. S3. Similar chemistry is also applicable to the bromide–iodide conversion process. It is noted that the bromide part and the chloride part show a weak contrast difference even in the optical image (Fig. 1*C*). The PL emission of the individual nanowires after reaction was examined. Fig. 1 *D*–*G* shows the optical images and PL spectra of the Br–Cl and Br–I partially exchanged nanowires, respectively. Both nanowires feature two-color emissions with a clear, sharp interface. In the Br–Cl exchange sample, the blue part has an emission peak centered at 420 nm, suggesting a complete conversion from $CsPbBr_3$ to $CsPbCl_3$, whereas in the Br–I exchange case, the red region shows an emission peak centered at 655 nm, corresponding to ∼80% Br–I conversion (24). Notably, there are no additional emission peaks between the two major peaks in the PL spectra, which means the interface of the junction is relatively sharp with no significant interdiffusion of the Br^- and Cl^-/I^- ions. Such high-quality junction is important for electronic device applications.

The elemental distribution and morphology of the nanowires after anion exchange was examined by scanning electron microscopy (SEM). As shown in Fig. 2*A*, the SEM energy-dispersive X-ray spectroscopy (EDS) mapping on a heterojunction nanowire shows a clear interface between the bromide section (green) and chloride section (blue), whereas other elements such as lead (purple) and cesium (yellow) are uniformly distributed within the whole nanowire. Note the weak chlorine signal in the bromide part is likely from lead, because the Pb M shell has a similar energy to that of the Cl K shell (see *SI Appendix*, Fig. S4 for the EDS spectrum and more explanation). Fig. 2*B* shows the relative bromide and chloride concentration profiles along the nanowire. Both elements are spatially confined. Dramatic changes of Cl and Br concentrations at the interface region are observed. Another SEM image (*SI Appendix*, Fig. S5) shows that the nanowire morphology is well-preserved upon chemical conversion. The $CsPbBr_3$ part features a width of 741 nm while the width of the $CsPbCl_3$ part shrinks to 714 nm; the 3.8% change in the nanowire width is consistent with the difference of the lattice constant between the bromide (orthorhombic: a = 8.207 Å, b = 8.255 Å, c = 11.759 Å, Z = 4, V/Z = 199.16) and chloride (tetragonal: a = b = 5.584 Å, c = 5.623 Å, Z = 1, V/Z = 175.33) room temperature phases (nanowire growth direction is [110], ref. 25).

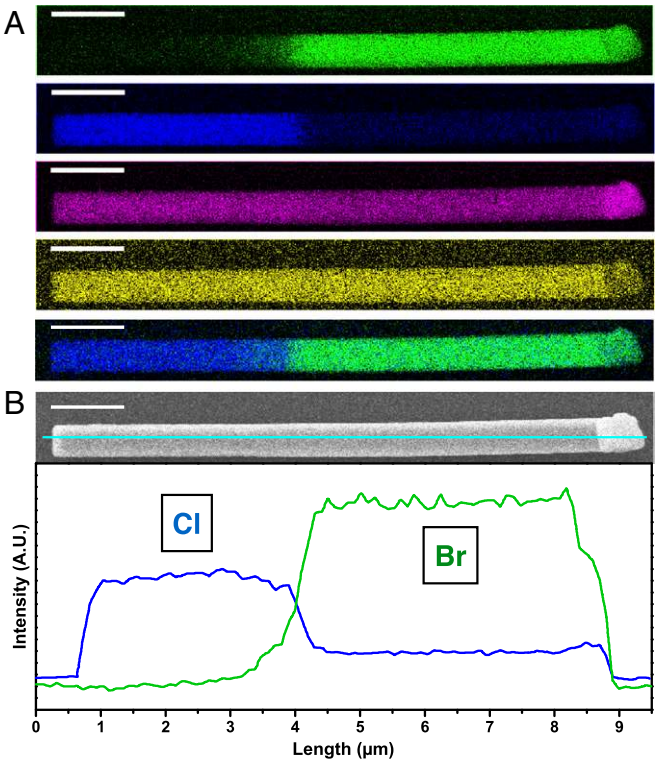

Fig. 2. Elemental distribution of the heterojunction nanowire. (*A*) SEM EDS elemental mapping on the heterojunction nanowire. Green: bromine; blue: chlorine; purple: lead; yellow: cesium. (*B*) The SEM image of the heterojunction nanowire and the corresponding chlorine and bromine distribution profile along the nanowire. (Scale bars, 1 μm.)

The local electronic structure of the junction was examined by scanning Kelvin probe force microscopy (KPFM) combined with atomic force microscopy (AFM). Fig. 3*A* shows the 3D AFM topographic image of a partially converted nanowire on SiO_2/Si. The nanowire profile reveals heights of 523 and 504 nm for the $CsPbBr_3$ and $CsPbCl_3$ parts (Fig. 3*B* and *SI Appendix*, Fig. S6*A*), respectively, which again agrees well with the theoretically expected relative dimensional change. The observed gradual height transition occurring over ∼1 μm is inherently linked to the release of lattice-mismatch-induced strain at the electronic junction (note: the height profile transition width is not necessarily equal to the junction width). No grain boundaries or cracks in the crystal were observed in the AFM and SEM images, indicating that the nanowire remains single crystalline with the heterojunction being probably of epitaxial nature. However, further study using high-resolution transmission electron microscopy is needed to elucidate the underlying atomic structure of the heterojunction. Upon chemical conversion, the nanowire maintains its high structural quality and very low surface roughness (rms< 5 nm). Fig. 3 *C* and *D* shows the nanowire's 3D KPFM surface potential map and the corresponding 2D potential profile. In response to the compositional variation within the nanowire, a sharp relative surface potential change of ∼190 meV is observed across the heterojunction interface. Detailed electronic characterization of various heterojunction nanowires consistently revealed higher surface potential values for the $CsPbBr_3$ part relative to the $CsPbCl_3$ part (*SI Appendix*, Fig. S7), indicating a shallower Fermi level in $CsPbBr_3$. These findings demonstrate the feasibility of our approach to create interfaces of distinct compositional and electronic properties at high spatial control. The workfunction values of pristine $CsPbBr_3$ and $CsPbCl_3$ nanowires were quantitatively determined by KPFM measurements (*SI Appendix*, Figs. S8 and S9). As illustrated in Fig. 3*E*, we obtain workfunction values of 4.77 ± 0.03 eV for $CsPbBr_3$ and 4.93 ± 0.03 eV for $CsPbCl_3$, respectively. The suggested band alignment at the heterojunction is illustrated in Fig. 3*F* (28, 29). The band structure can be further tuned by controlling the composition and doping, which opens up the possibility for electronic device applications. Moreover, we demonstrate multijunctions in a single nanowire. Fig. 3*G* shows the 3D KPFM surface potential map and corresponding 2D potential profile of a nanowire comprising four heterojunctions with each segment of ∼3 μm (see *SI Appendix*, Fig. S6*B* for topography). Similar to the single heterojunction nanowire, the $CsPbBr_3$ and $CsPbCl_3$ regions feature distinct electronic characteristics.

The sharp electronic interface of the heterojunctions allows us to reduce the feature size, and the robustness of the nanowire allows us to introduce additional fabrication steps to create multicolor heterojunctions. To study the spatially resolved patterns, confocal PL mapping with high spatial resolution was used, and the results are summarized in Fig. 4. For the Br–Cl exchanged nanowire, the confocal PL mapping results (Fig. 4 *A*–*C*) are

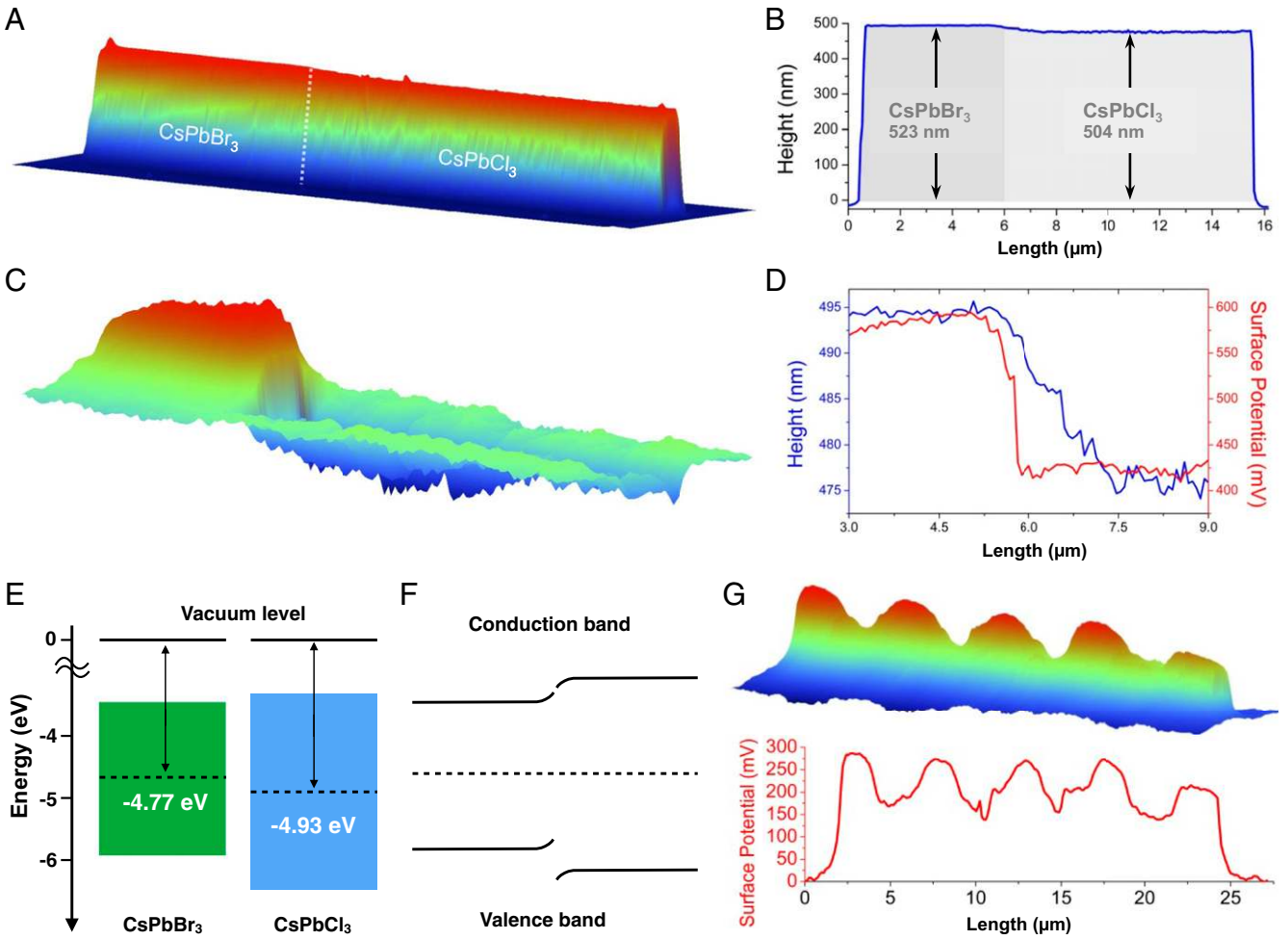

Fig. 3. Morphology and electronic structure of the heterojunction. (*A*) Three-dimensional AFM topographical view of a typical Br–Cl exchanged heterojunction nanowire on SiO_2/Si. The white dashed line indicates the interface of the bromide (*Left*) and chloride (*Right*) parts. (*B*) The corresponding height profile of the heterojunction nanowire. (*C*) Three-dimensional view of the KPFM surface potential mapping of the heterojunction nanowire. (*D*) The corresponding potential profile across the junction interface (red curve) with the corresponding AFM height profile (blue curve). (*E*) Work functions of the pure $CsPbBr_3$ and $CsPbCl_3$ nanowires determined by quantitative KPFM. The green and blue squares indicate the band gap of the pure $CsPbBr_3$ and $CsPbCl_3$, respectively. (*F*) Proposed band alignment of the $CsPbBr_3$–$CsPbCl_3$ heterojunction nanowire. (*G*) Three-dimensional view of the KPFM surface potential mapping of a multisegment heterojunction nanowire (each segment is ∼3 μm long) and the corresponding potential profile along the nanowire.

similar to the PL image in Fig. 1*D*, with a better-resolved interface. As shown in *SI Appendix*, Fig. S10, the length of the exposed area and the covered area prior conversion are 10.8 and 8.7 μm long, respectively, whereas after the conversion the lengths for the chloride and bromide regions changed to 10.8 and 8.6 μm (the dark region in between is around 100 nm). This demonstrates that the reaction is well defined at the exposed area with the PMMA coating effectively protecting the area underneath. The spectral scan on a Br–Cl exchanged nanowire shows almost no PL emission from 450 to 480 nm and a sharp switching from blue to green emissions (*SI Appendix*, Fig. S11). The junction width is smaller than 500 nm, which is consistent with the SEM EDS mapping as well as the distinct surface potential change in the KPFM measurement. We then created multiple junctions with pixel size (open window of PMMA by e-beam) of ∼1 μm on a nanowire (Fig. 4 *D*–*F*). After conversion, the superlattice structure can be clearly resolved. Such a feature cannot be resolved very well via the PL imaging measurement (*SI Appendix*, Fig. S12). We further decrease the pixel size to less than 500 nm, and the features can still be resolved (Fig. 4 *G*–*I*). However, attempts to further decrease the pixel size to 200 nm were not successful (*SI Appendix*, Fig. S13). The resolution is probably limited by the instrument (diffraction limit) or the interdiffusion of anions within such a small area. Next, based on the two-color heterostructure, another fabrication-conversion step was added: a red–green–blue three-color heterojunction was achieved, as shown in Fig. 4*J*. In principle, the emission wavelength of the red and blue parts is tunable by varying the conversion degree, and the relative intensity of each color can be tuned by varying the pixel size of each segment. Such color-tunable perovskite heterostructures provide an ideal platform for full-color displays and solid-state lighting (30–33). The spectral scan on the three-color nanowire shows two sharp junctions at the interfaces (*SI Appendix*, Fig. S14). Finally, we demonstrate high-resolution arbitrary patterns on $CsPbBr_3$ perovskite plates using the spatial-controlled anion-exchange chemistry. As shown in Fig. 4 *K*–*M*, strips, an arrow target, and a University of California, Berkeley, logo can be written on the $CsPbBr_3$ plates.

The nanowire heterojunctions show good stability. After being stored in a nitrogen atmosphere for 1 wk, confocal PL mapping of the partial bromide partial chloride nanowire and the superlattice nanowire exhibited PL emissions and sharp junctions very similar to the initial states (*SI Appendix*, Fig. S15). These results indicate that the anion interdiffusion occurs much more slowly across the heterojunction compared with the exchange reaction at the solid–liquid

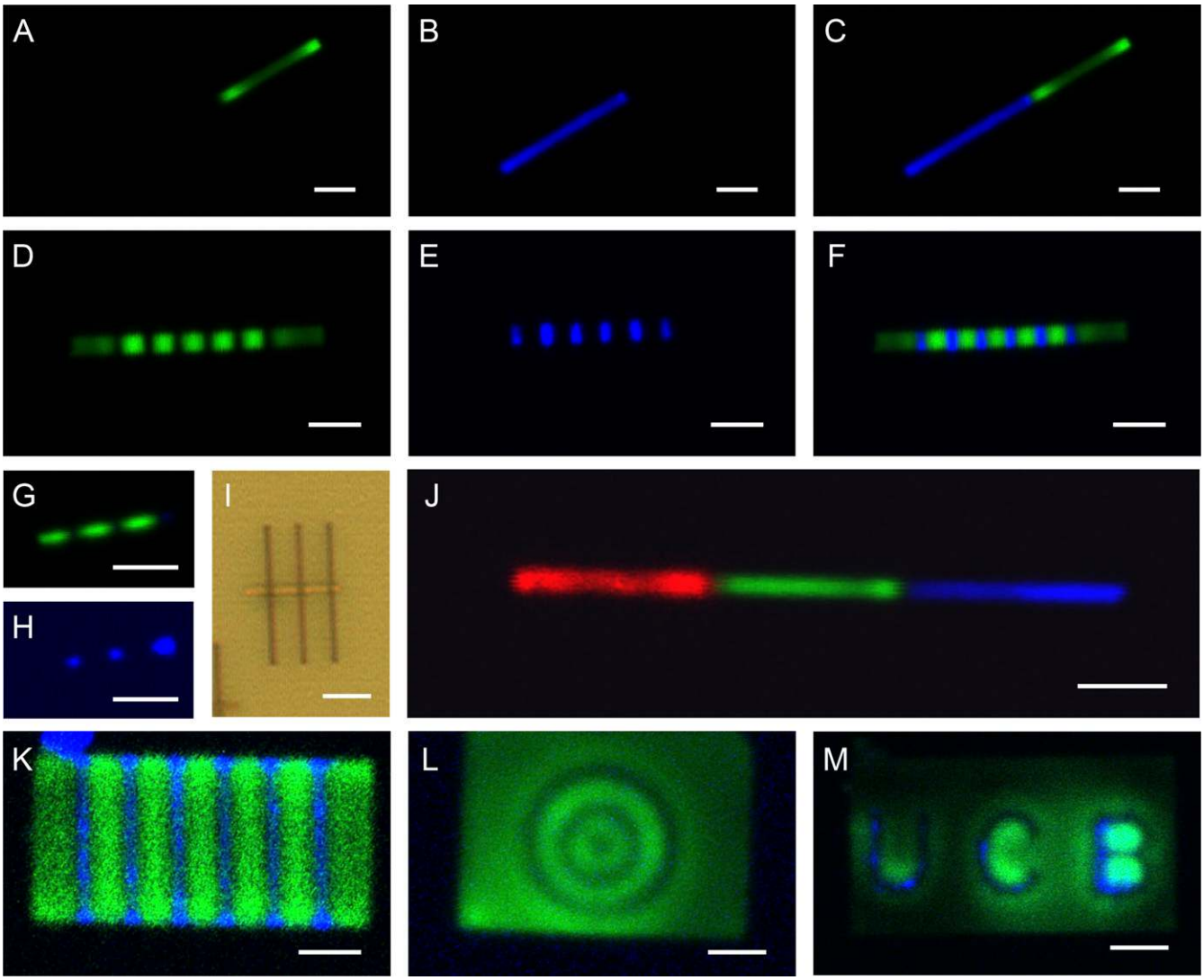

Fig. 4. Confocal PL mapping of different types of heterojunctions. (*A–C*) Confocal PL mapping of a partial bromide partial chloride nanowire. Blue represents emission from 410 to 450 nm. Green represents emission from 500 to 550 nm. (*D–F*) Confocal PL mapping of a bromide–chloride superlattice nanowire with pixel size of below 1 μm. (*G–I*) Confocal PL mapping and optical image of a bromide–chloride superlattice nanowire with pixel size of below 500 nm. (*J*) Confocal PL mapping of a three-color heterojunction nanowire. Blue represents emission from 410 to 450 nm. Green represents emission from 500 to 550 nm. Red represents emission from 580 to 640 nm. (*K–M*) Confocal PL mapping of different patterns on $CsPbBr_3$ plates. (Scale bars, 3 μm.)

interface of the exposed area. There are two possible reasons: First, at the exposed area, more vacancies may be introduced from the solid–liquid interface due to the interaction between the perovskite solid and the precursor molecules and ions in the solution; furthermore, higher vacancy concentration in the exposed region leads to faster ion migration and exchange reaction (12, 18). Second, the ion migration may have higher activation energy along the nanowire growth direction, and thus anion exchange/migration proceeds slightly slower along this direction (34).

Conclusions

In summary, our results suggest that the anion-exchange chemistry combined with nanofabrication is a powerful tool to create high-quality semiconductor heterojunctions and patterns at the nanometer scale. The solid-state ion diffusion rate in halide perovskite is much slower than expected. The halide perovskite nanowire heterojunction provides an ideal platform for fundamental studies and technological applications. For example, multicolor lasers or LEDs could be made using such localized heterojunctions; quantitative interdiffusion and ion migration dynamics could be examined at elevated temperatures, etc. With deeper understanding of these heterojunctions, halide perovskites may find practical applications in large-scale electronic circuit, information storage, and full color displays, in addition to the current interest in photovoltaic cells.

Materials and Methods

Additional details regarding the materials and methods may be found in the *SI Appendix*.

Anion Exchange of $CsPbBr_3$ Nanowires. To convert the $CsPbBr_3$ to $CsPbCl_3$, 10 mg of oleylammonium chloride was dissolved in 10 mg of 1-Octadecene (ODE) to make the conversion solution. Individual $CsPbBr_3$ nanowires were transferred onto a clean Si/SiO_2 substrate using a nanomanipulator. The chip with nanowires was immersed into the conversion solution at room temperature for 16 h for complete conversion. Then, the chip was taken out from the solution and washed with chlorobenzene twice and hexanes once to remove the extra salts left on the chip. The reaction dynamics can be tracked in situ by monitoring the PL emission of an individual nanowire. To convert the $CsPbBr_3$ to $CsPbI_3$, 10 mg of oleylammonium iodide was dissolved in 10 mg of ODE to make the conversion solution and the reaction was carried out at room temperature for 4 h.

Fabrication of the Nanowire Heterojunctions. To fabricate heterojunction devices, the as-grown nanowires were first transferred onto a 300-nm SiO_2-coated Si substrate by a micromanipulator. The substrate was then spin-coated with PMMA, and baked at 130 °C for 6 min. E-beam lithography (EBL) was performed in a Crestec CABL-9510CC High-Resolution Electron Beam Lithography System with acceleration voltage of 50 keV and beam current of 500 pA. After EBL, the substrate was dipped into developer (methyl isobutyl ketone:isopropyl alcohol = 1:3) for 60 s followed by washing in isopropyl alcohol for another 20 s. The developer and isopropyl alcohol were dried with molecular sieves (Sigma-Aldrich) to remove water molecules. Subsequently, the nanowires with partially coated PMMA were immersed into the conversion solution. The conversion reaction was carried out using the same recipe as described above. After conversion, the PMMA mask was removed by dipping the substrate into chlorobenzene and hexanes, respectively.

Note, although different ways of carrying out the anion-exchange reaction have been reported, none of them are applicable here. For example, more polar solvents such as toluene, chlorobenzene, or isopropanol can either dissolve the PMMA mask and/or damage the nanowire. Even with ODE, higher temperature will also damage the nanowire morphology. For vapor-phase conversion, heating at over 100 °C is necessary to evaporate the organic halide precursors, which may also damage the PMMA layer. Therefore, a nonpolar solvent, such as ODE, is critical. To dissolve the halide precursor in such nonpolar solvent, an ammonium cation with a long carbon chain is necessary.

AFM and Scanning KPFM Measurements. AFM and scanning KPFM measurements were performed on an AFM system (MFP-3D Asylum Research, Oxford Instruments) equipped with an acoustic isolation chamber (AEK 2002). The samples were transferred from the preparation glovebox into the AFM chamber operated in nitrogen atmosphere. The AFM/KPFM measurements were performed at room temperature using conductive platinum-coated silicon cantilevers (Olympus AC240TM-R3). KPFM measurements were performed in a two-pass mode: the first scan for topographical imaging in ac mode followed by the interleave mode, in which the conductive tip was lifted with constant separation relative to the specimen surface while acquiring the contact potential difference, V_{CPD}. To achieve the highest lateral resolution, the influence of the lift height on the measured surface potential was carefully checked by surface potential vs. z spectroscopy, whereas only a minor influence of the lift height on the measured CPD signals was observed in the delta lift height region of −10–30 nm. Accordingly, for all surface potential measurements the delta lift height was set to result in a tip apex–surface distance of ∼20 nm. An ac bias of 3 V amplitude at the first contact resonance frequency and a dc bias of 1 V was applied to the conductive probe. All measurements were performed at low scan rate of 0.2 Hz at a resolution of 256 × 256 pixels. Ambient light is minimized by the AFM isolation chamber, whereas a low-intensity ∼5-mW IR diode (860 nm) is used to detect probe deflection.

Confocal PL Mapping. Confocal PL mapping was performed using an Olympus IX83 laser scanning confocal microscope with a 40× 0.95 N.A. objective and a 405-nm laser excitation source. All images were 512 × 512 pixels collected at 10 ms per line. $CsPbCl_3$, $CsPbBr_3$, and $CsPbI_3$ emission were collected over a spectra range of 410–450, 500–550, and 580–640 nm, respectively, using an emission grating. Multichannel images were collected in series or simultaneously using either a 473- or 560-nm dichroic. Lambda scans were performed by collecting a series of images while scanning the emission grating in 10-nm spectral windows to vary the collected wavelength range.

ACKNOWLEDGMENTS. We thank Dr. Dylan Lu and Dr. Chong Liu for the help with the PL and KPFM measurements, and Dr. Yehonadav Bekenstein and Andrew B. Wong for helpful discussions. This work was supported by the US Department of Energy, Office of Science, Basic Energy Sciences, Materials Sciences and Engineering Division under Contract DE-AC02-05CH11231 (Physical Chemistry of Inorganic Nanostructures KC3103). M.L. acknowledges the fellowship support from Suzhou Industrial Park. C.S.K. acknowledges support by the Alexander von Humboldt Foundation. C.G.B. acknowledges a National Science Foundation Graduate Research Fellowship (DGE 1106400), and N.S.G. acknowledges a Packard Fellowship for Science and Engineering, a Camille Dreyfus Teacher-Scholar Award, and an Alfred P. Sloan Research Fellowship.

1. Lee MM, Teuscher J, Miyasaka T, Murakami TN, Snaith HJ (2012) Efficient hybrid solar cells based on meso-superstructured organometal halide perovskites. *Science* 338: 643–647.
2. Burschka J, et al. (2013) Sequential deposition as a route to high-performance perovskite-sensitized solar cells. *Nature* 499:316–319.
3. Zhou H, et al. (2014) Photovoltaics. Interface engineering of highly efficient perovskite solar cells. *Science* 345:542–546.
4. Dong Q, et al. (2015) Solar cells. Electron-hole diffusion lengths > 175 μm in solution-grown CH3NH3PbI3 single crystals. *Science* 347:967–970.
5. Jeon NJ, et al. (2015) Compositional engineering of perovskite materials for high-performance solar cells. *Nature* 517:476–480.
6. Protesescu L, et al. (2015) Nanocrystals of cesium lead halide perovskites (CsPbX3, X= Cl, Br, and I): Novel optoelectronic materials showing bright emission with wide color gamut. *Nano Lett* 15:3692–3696.
7. Ning Z, et al. (2015) Quantum-dot-in-perovskite solids. *Nature* 523:324–328.
8. Zhang D, Eaton SW, Yu Y, Dou L, Yang P (2015) Solution-phase synthesis of cesium lead halide perovskite nanowires. *J Am Chem Soc* 137:9230–9233.
9. Dou L, et al. (2015) Atomically thin two-dimensional organic-inorganic hybrid perovskites. *Science* 349:1518–1521.
10. Akkerman QA, et al. (2016) Solution synthesis approach to colloidal cesium lead halide perovskite nanoplatelets with monolayer-level thickness control. *J Am Chem Soc* 138:1010–1016.
11. Akkerman QA, et al. (2015) Tuning the optical properties of cesium lead halide perovskite nanocrystals by anion exchange reactions. *J Am Chem Soc* 137:10276–10281.
12. Nedelcu G, et al. (2015) Fast anion-exchange in highly luminescent nanocrystals of cesium lead halide perovskites (CsPbX3, X= Cl, Br, I). *Nano Lett* 15:5635–5640.
13. Wong AB, et al. (2015) Growth and anion exchange conversion of CH3NH3PbX3 nanorod arrays for light-emitting diodes. *Nano Lett* 15:5519–5524.
14. Pellet N, Teuscher J, Maier J, Grätzel M (2015) Transforming hybrid organic inorganic perovskites by rapid halide exchange. *Chem Mater* 27:2181–2188.
15. Zhang D, et al. (2016) Synthesis of composition tunable and highly luminescent cesium lead halide nanowires through anion-exchange reactions. *J Am Chem Soc* 138: 7236–7239.
16. Akamatsu K, Ikeda S, Nawafune H, Yanagimoto H (2004) Direct patterning of copper on polyimide using ion exchangeable surface templates generated by site-selective surface modification. *J Am Chem Soc* 126:10822–10823.
17. Lahav M, et al. (2006) Patterning of poly (acrylic acid) by ionic exchange reactions in microfluidic channels. *Adv Mater* 18:3174–3178.
18. Robinson RD, et al. (2007) Spontaneous superlattice formation in nanorods through partial cation exchange. *Science* 317:355–358.
19. Miszta K, et al. (2014) Nanocrystal film patterning by inhibiting cation exchange via electron-beam or X-ray lithography. *Nano Lett* 14:2116–2122.
20. Palazon F, Akkerman QA, Prato M, Manna L (2016) X-ray lithography on perovskite nanocrystals films: From patterning with anion-exchange reactions to enhanced stability in air and water. *ACS Nano* 10:1224–1230.
21. Cui Y, Wei Q, Park H, Lieber CM (2001) Nanowire nanosensors for highly sensitive and selective detection of biological and chemical species. *Science* 293:1289–1292.
22. Li Y, Qian F, Xiang J, Lieber CM (2006) Nanowire electronic and optoelectronic devices. *Mater Today* 9:18–27.
23. Yan R, et al. (2011) Nanowire-based single-cell endoscopy. *Nat Nanotechnol* 7: 191–196.
24. Dasgupta NP, et al. (2014) 25th anniversary article: Semiconductor nanowires–synthesis, characterization, and applications. *Adv Mater* 26:2137–2184.
25. Eaton SW, et al. (2016) Lasing in robust cesium lead halide perovskite nanowires. *Proc Natl Acad Sci USA* 113:1993–1998.
26. Zhu H, et al. (2015) Lead halide perovskite nanowire lasers with low lasing thresholds and high quality factors. *Nat Mater* 14:636–642.
27. Son DH, Hughes SM, Yin Y, Paul Alivisatos A (2004) Cation exchange reactions in ionic nanocrystals. *Science* 306:1009–1012.
28. Li G, et al. (2016) Highly efficient perovskite nanocrystal light-emitting diodes enabled by a universal crosslinking method. *Adv Mater* 28:3528–3534.
29. Van Le Q, Park M, Sohn W, Jang HW, Kim SY (2017) Investigation of energy levels and crystal structures of cesium lead halides and their application in full-color light-emitting diodes. *Adv Electron Mater* 3:1600448.
30. Tan Z-K, et al. (2014) Bright light-emitting diodes based on organometal halide perovskite. *Nat Nanotechnol* 9:687–692.
31. Shirasaki Y, Supran GJ, Bawendi MG, Bulović V (2013) Emergence of colloidal quantum-dot light-emitting technologies. *Nat Photonics* 7:13–23.
32. D'Andrade BW, Forrest SR (2004) White organic light-emitting devices for solid-state lighting. *Adv Mater* 16:1585–1595.
33. Fan F, Turkdogan S, Liu Z, Shelhammer D, Ning CZ (2015) A monolithic white laser. *Nat Nanotechnol* 10:796–803.
34. Amin R, Balaya P, Maier J (2007) Anisotropy of electronic and ionic transport in $LiFePO_4$ single crystals. *Electrochem Solid-State Lett* 10:A13–A16.